Research Article

Sergey S. Khrapov and Alexander V. Khoperskov*

Retrograde infall of the intergalactic gas onto S-galaxy and activity of galactic nuclei

https://doi.org/10.1515/astro-2022-0231 received August 24, 2023; accepted January 22, 2024

Abstract: We present the results of numerical simulations focused on the accretion of intergalactic gas onto a gas-rich S-type disc galaxy. Our investigation explores the conditions favouring the emergence of counterrotating stellar and gaseous components within the galaxy, leading to the inflow of gas towards the central kiloparsec of the galaxy. Notably, we find that the most substantial reservoir of gas, serving as fuel for galactic nucleus activity, resides within the central region during the retrograde infall of gas at an incident angle of approximately 20° relative to the galactic plane. Departures from this angle significantly diminish the gas flow rate towards the galactic centre. Conversely, the prograde infall of intergalactic gas makes a marginal contribution to the gas content in the central region and cannot supply fuel to the active galactic nucleus. An intriguing characteristic of the observed retrograde impact is the emergence of a rotating polar ring at the galaxy's periphery, primarily originating from intergalactic gas.

Keywords: galaxies, gas accretion, counterrotation, numerical simulation

1 Introduction

The galaxy formation process occurs within the gravitational potential of massive dark matter halos, a result of major and minor mergers involving systems of various properties. The growth of galaxies is driven by the substantial accumulation of gas, serving as the source for subsequent star formation. Hence, the characteristics of galactic stellar populations are intricately linked to the parameters of gas accretion.

There is a great variety of galaxies with misaligned kinematics of different stellar populations. Galaxies exhibiting counterrotation, where the rotational directions of gas and stars are opposing, hold a special significance in the field (Li *et al.* 2021, Katkov *et al.* 2022, Proshina *et al.* 2016). It is worth emphasizing that counterrotating discs attract attention even within large-scale cosmological models. For instance, data stemming from IllustrisTNG100 simulations reveal kinematically misaligned discs spanning a broad spectrum of galactic parameters (Starkenburg *et al.* 2019, Duckworth *et al.* 2020a, Khoperskov *et al.* 2021, Lu *et al.* 2021).

In recent years, the count of observed galaxies displaying counterrotation or some form of kinematic misalignment between their stellar and gas components has been on the rise. These phenomena are no longer as exotic as the initial discoveries suggested (Franx and Illingworth 1988). A specific class of such systems comprises galaxies with a clear misalignment in the kinematics of various stellar components, for instance, PGC 66551 and NGC 254 (Katkov *et al.* 2022, 2023). This phenomenon arises because the kinematic characteristics of the original gas are preserved during the star formation process.

Stellar discs with such kinematics in galaxies of different morphological types are associated with close interactions and mergers, which are most effective in dense environments. The kinematic reversal is found in PGC 046832, which is the central object of the cluster Abell 3556 (Brok et al. 2021). Generally speaking, mechanisms for the formation of counterrotating galaxies include a retrograde infall of gas onto the disc (Osman and Bekki 2017, Khoperskov et al. 2021) and a minor merger of a gas-rich dwarf galaxy (Di Matteo et al. 2008, Saburova et al. 2018, Bassett et al. 2017). As a result, the differences in the kinematics of stellar populations are often imprinted in the diverse age and chemical composition of the two stellar components (Pizzella et al. 2014, Nedelchev et al. 2019). Therefore, determining the specific mechanism responsible for the formation of misaligned stellar components in different galaxies can be accomplished by analysing its chemical composition, as outlined by Zinchenko (2023).

^{*} Corresponding author: Alexander V. Khoperskov, Department of Information Systems and Computer Modeling, Volgograd State University, Volgograd, Russia, e-mail: khoperskov@volsu.ru Sergey S. Khrapov: Department of Information Systems and Computer Modeling, Volgograd State University, Volgograd, Russia, e-mail: khrapov@volsu.ru

It is crucial to highlight that the accreting gas becomes essential for both star formation and central activity in early-type galaxies once their internal gas reserves are depleted. The fraction of lenticular galaxies displaying counterrotation between their gas and stellar components stands at approximately 30%. Recent observational data suggest a relative increase in the prevalence of such objects as ongoing research unfolds (Katkov *et al.* 2014, 2023, Raimundo 2021). The emergence of gas in early-type galaxies is commonly interpreted as a consequence of mergers and/or cold accretion (Davis *et al.* 2011). In contrast, the occurrence of counterrotation between gas and stars in late-type galaxies is around 10% due to the complicating presence of the original gaseous disc, which hampers the detection of misaligned kinematics (Pizzella *et al.* 2004).

Instances of misaligned kinematics or kinematic reversals can be observed in the context of active galactic nuclei (AGN), as exemplified by IC 1459 (Franx and Illingworth 1988) and NGC 5077 (Raimundo 2021). Analysing various samples enables the identification of kinematically distinct galactic cores (Krajnovic *et al.* 2011, Raimundo 2021, Ebrova *et al.* 2021), with IC 1459 serving as one of the prototypes in this regard (Franx and Illingworth 1988).

Counterrotation can enhance the conditions conducive to the activity of AGN by augmenting the inflow of gas towards the supermassive black hole. This phenomenon is substantiated by numerical simulations (Negri *et al.* 2014, Starkenburg *et al.* 2019). Recent analyses underscore the effectiveness of fuelling such nuclei, both on an individual galaxy basis (Gnilka *et al.* 2020, Raimundo 2021) and across larger datasets (Raimundo *et al.* 2023). One intriguing attribute of gas distribution in some Seyfert galaxies is the presence of nearly non-rotating ionized gas within the central region, as exemplified by NGC 5899 (Bianchin *et al.* 2022).

Traces of counterrotation in disc are a fairly common phenomenon both in early type galaxies (about 10–15%) and in blue galaxies (~2%) (Barrera-Ballesteros *et al.* 2015, Chen *et al.* 2016). The central regions of late-type counterrotating galaxies exhibit increased rates of star formation due to the additional flow of gas into the centre. Major mergers of two spiral galaxies of comparable mass result in elliptical or lenticular galaxies with a kinematically distinct core (Bois *et al.* 2011).

A detailed analysis of the dynamics of counterrotating galaxies based on the Illustris TNG100 cosmological simulation data formed the basis for the scenario of their formation due to retrograde gas accretion processes onto a gas-rich disc galaxy (Khoperskov *et al.* 2021). The sample of 25 galaxies included objects with two counterrotating stellar discs and a gaseous component that rotates against

one of the stellar discs. It was demonstrated that the counterrotation of stars in galaxies results from star formation in a gaseous disc accreted from the outer reservoir. This counterrotating gaseous component completely replaces the pre-existing gaseous disc, so the initial stage of the formation of counterrotating galaxies involves a significant loss of gas by the galaxy (Khoperskov et al. 2021). In addition, some of these galaxies look like polar ring galaxies (PRGs) as a result of gas accretion, which indicates a single mechanism for transporting gas to the centre and the formation of misaligned kinematics in the disc along with the outer polar ring. It must be emphasized that the occurrence of PRGs among nearby galaxies is approximately 0.1% (Moiseev et al. 2011, Reshetnikov et al. 2011, Reshetnikov and Mosenkov 2019) or even ~1% (Mosenkov et al. 2023), which, however, depends on the sample.

The connection between AGN and polar rings is clearly visible in observational data (Smirnov and Reshetnikov 2020, Hauschild *et al.* 2022). For example, SDSS data show an increased occurrence of central activity among PRGs. The edge-on galaxy NGC 4111 is an interesting example where the central activity is fed by gas directly from the inner polar ring with a diameter of only 450 pc (Hauschild *et al.* 2022).

Thus, counterrotations in the disc, central activity, and polar rings may be manifestations of a single process of minor merging of a gas-rich galaxy or accretion of a dense gas filament. There are numerical studies of such mergings aimed at identifying the mechanisms of the formation of multi-spin systems, including rings of different orientations and strong bends of discs (Bekki 1997, Bournaud and Combes 2003, Mapelli et al. 2015, Reshetnikov and Sotnikova 1997). The forming polar rings consist of gas and stars of a dwarf galaxy, the process of destruction of which takes a long time. The term "polar rings" traditionally includes systems with some deviation from the angle $\Theta = 90^{\circ}$ between the ring and the host disc (tilted ring/disc or warped ring/disc) (Moiseev 2008, Finkelman et al. 2011, Khoperskov et al. 2014, Merkulova et al. 2012, Mosenkov et al. 2022). The Illustris TNG50 simulations allow us to study the mechanisms of formation of PRGs and the evolution of the angle of polar rings (Smirnov et al. 2023).

Our research is dedicated to conducting an in-depth examination of the process involving the replacement of a galaxy's gaseous disc. This replacement is contingent upon the angle of incidence of retrograde intergalactic gas infall. The primary objective of this study is to establish the correlation between gas accretion onto the galactic disc and the efficiency of delivering gas to the central region, thereby sustaining an active galactic nucleus. The comprehensive problem formulation, the underlying

mathematical model, and the numerical algorithm are expounded upon in Section 2. The outcomes of our numerical simulations are presented in Section 3, followed by a discussion of conclusions in Section 4. An accreting gas intergalactic filament can also generate an outer rotating ring of gas around the host disc galaxy, which is located in different planes. We briefly discuss this phenomenon of polar/tilted rings formed from the portion of gas that ends up outside the galactic disc after the interaction (Section 3).

2 Model and initial setup

The parameters of the main galaxy model are typical for large galaxies such as the Milky Way, with a maximum rotation velocity of about 220 km/s and a substantial amount of gas in the disc, which extends for about 20 kpc. The optical radius of the galaxy coincides with the size of the stellar disc and is equal to 10 kpc. We use the basic model of the host galaxy described by Khoperskov et al. (2021, 2024), Khrapov et al. (2021). The differences are related to the radial profiles of the stellar velocity dispersion and the thickness of the stellar disc in order to consider a gravitationally stable stellar-gaseous disc and exclude the development of spiral arms and a bar before the gas accretion. We also consider a spherically symmetric dark halo density distribution to avoid the formation of a spiral/bar structure at the initial stage (Butenko et al. 2015, 2022).

The accreting intergalactic gas in the numerical model is given by eight spheroidal gas clouds at the initial time (Figure 1). These gaseous clumps are located at a distance of more than 30 kpc, far beyond the optical radius of the galaxy, and move along a parabolic trajectory that crosses the disc of the main galaxy. The initial inclination of the trajectory of gas clouds relative to the galactic plane equals Θ_g (the angle $\Theta_g = 0$ corresponds to motion in the disc plane). Their initial velocity of 0.8 of the circular velocity at a given radius ensures the infall of gas into the central zone of the galaxy.

We consider both the retrograde infall of the gas and the direct infall with respect to the initial rotation of the galaxy, which are determined by the initial parameters of the orbit of the intergalactic gas flow. The evolution of all components is calculated over 7 billion years. The structure and kinematics of the gaseous and stellar subsystems are modelled to understand the mechanism of gas delivery to the central kiloparsec of the galaxy, which is one of the key problems of the galactic nuclei activity.

2.1 Mathematical model

The equations of motion of gravitationally interacting gaseous and collisionless particles have the following form:

$$\frac{\mathrm{d}^{2}\mathbf{r}_{i}}{\mathrm{d}t^{2}} = \begin{cases}
-\frac{\nabla p_{i}}{\varrho_{i}} + \mathbf{f}_{i}^{h} + \sum_{j=1, j \neq i}^{N} \mathbf{f}_{ij}, & 0 \leq i < N_{g}, \\
\mathbf{f}_{i}^{h} + \sum_{j=1, j \neq i}^{N} \mathbf{f}_{ij}, & Ng \leq i < N = Ng + N_{*},
\end{cases}$$
(1)

where the radius vector $\mathbf{r}_i(t) = \int \mathbf{v}_i dt$ determines the position of the *i*th particle in space, \mathbf{v}_i is the velocity of the *i*th particle, and ϱ_i and p_i are the volume density and gas

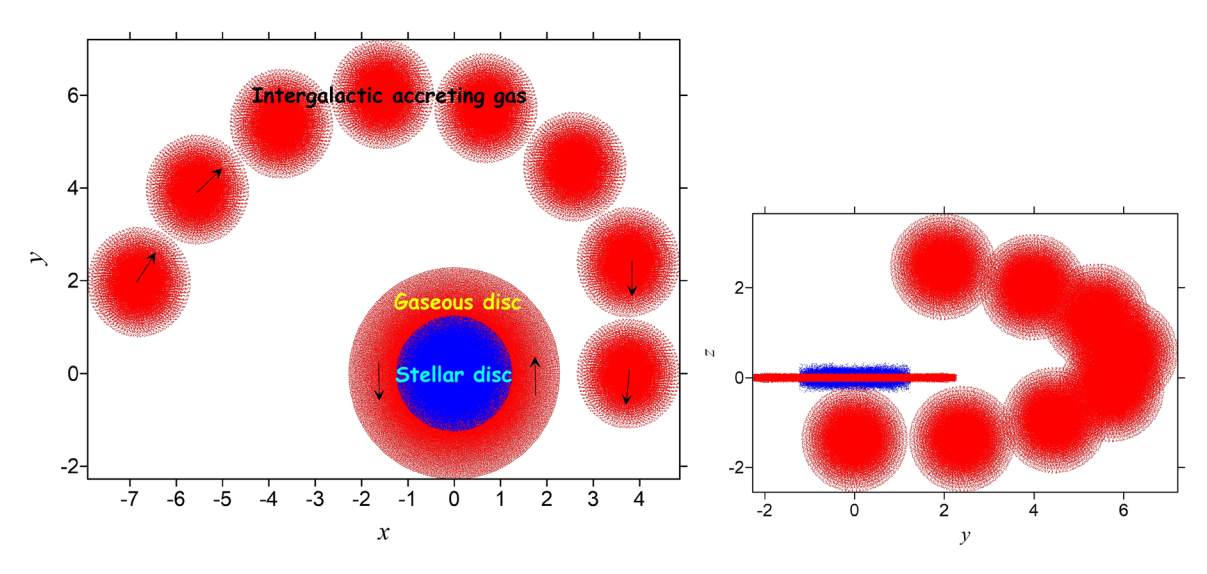


Figure 1: Scheme of intergalactic gas infall onto S-galaxy in computational experiments.

pressure of the *i*th smoothed–particle hydrodynamics (SPH) particle, respectively. The gravitational interaction between the *i*th and *j*th particles is calculated using the following formula:

$$\mathbf{f}_{ij} = -G \frac{m_j(\mathbf{r}_i - \mathbf{r}_j)}{[(\mathbf{r}_i - \mathbf{r}_j)^2 + \delta^2]^{3/2}},$$
 (2)

where G is the gravitational constant, m_j is the mass of the jth particle, and δ is the gravitational smoothing length at very short distances. The length δ for all components is the same and amounts to $\delta = 20$ pc.

The gas dynamics model also includes the equation of state of the gas $e = e(p, \varrho)$ and the conservation equation of specific internal energy e_i in the following form:

$$\frac{\mathrm{d}e_i}{\mathrm{d}t} = -\frac{p_i}{\varrho_i} \nabla \cdot \mathbf{v}_i + Q - \Lambda, \tag{3}$$

$$e_i = \frac{p_i}{(\gamma - 1)\varrho_i},\tag{4}$$

where γ is the adiabatic index, and Q and Λ are the heating and cooling functions, respectively.

The centre of the coordinate system (x, y, z) is placed in the initial centre of the galaxy. The disc is in the plane z = 0 (Figure 1). The initial rotation of the gas and stars in the galaxy is counterclockwise in the plane (x, y).

2.2 Numerical algorithm

The SPH approach defines the notation for the gas density of the *i*th gas particle, the equation of motion (1), and the equation for energy (3) in the form (Khrapov and Khoperskov 2017, Monaghan 1992):

$$\varrho_i = \varrho(\mathbf{r}_i) = \sum_{i=1}^{N_g} m_j \ W(|\mathbf{r}_i - \mathbf{r}_j|, h_{ij}), \tag{5}$$

$$\frac{\mathrm{d}\mathbf{v}_i}{\mathrm{d}t} = -\sum_{j=1,j\neq i}^{N_g} m_j \Pi_{ij} \nabla W_p(|\mathbf{r}_i - \mathbf{r}_j|, h_{ij})
+ \mathbf{f}_i^h + \sum_{j=1,j\neq i}^{N} \mathbf{f}_{ij},$$
(6)

$$\frac{\mathrm{d}e_i}{\mathrm{d}t} = \frac{1}{2} \sum_{j=1,j\neq i}^{N_g} m_j \ \Pi_{ij} \ (\mathbf{v}_i - \mathbf{v}_j) \cdot \nabla W_p(|\mathbf{r}_i - \mathbf{r}_j|, h_{ij}), \tag{7}$$

where W is the kernel function (Monaghan 2005), W_p is the smoothing kernel for calculating pressure forces (Muller et al. 2003), $\Pi_{ij} = \frac{p_i}{\rho_i^2} + \frac{p_j}{\rho_i^2} + \nu_{ij}^a$ is the symmetric SPH

approximation of the pressure force, v_{ij}^a is the artificial viscosity, and $h_{ij} = 0.5(h_i + h_j)$ is the effective smoothing length. The smoothing length of each i-particle depends on its mass and density as $h_i = 1.3(m_i/\varrho_i)^{1/3}$ (Khrapov and Khoperskov 2017, Monaghan 2005).

The second-order predictor-corrector scheme (leap-frog-method) is used for numerical integration of the differential Eqs (6) and (7). The calculation of gravitational forces based on the direct method "particle–particle" provides the best accuracy. We use two integration time steps to improve simulation performance. The step Δt , for calculating the gravitational interaction between particles $\mathbf{F}_i^{\mathrm{acc}}$ can significantly exceed the step Δt_g in the predictor–corrector scheme for gas dynamics ($\Delta t_g \ll \Delta t$.). Such choice requires correcting the particle velocities at each gravitational step to improve the accuracy of the predictor–corrector scheme:

$$\mathbf{v}_i(t + \Delta t_*) = \mathbf{v}_i(t^{(n+1)}) + \Delta \mathbf{v}_i^{\text{corr}}, \tag{8}$$

where

$$\Delta \mathbf{v}_i^{\text{corr}} = \frac{1}{2} (\Delta t_* - \Delta t_g^{(n)}) [\mathbf{F}_i^{\text{acc}}(t + \Delta t_*) - \mathbf{F}_i^{\text{acc}}(t)].$$

The numerical model of gas accretion onto the galactic disc is based on the system of joint equations of SPH and N-body dynamics. A detailed description of the computational model is given in Khrapov $et\ al.$ (2021), Khoperskov $et\ al.$ (2021), and Titov and Khoperskov (2022). The number of particles in the stellar and gas discs is $N_*=2^{19}$ and $N_g=2^{19}$, respectively. The gas flow is initially represented by the eight spheroidal clumps with the number of SPH particles $N_J=8\times 2^{17}=2^{20}$ in total. The SPH and N-body methods make it possible to track the origin of particles with complex dynamical mixing of several components. Therefore, we can measure the fraction of intergalactic gas in different subsystems at the end of the simulation.

The parameters of the galactic components in the basic model are listed below:

- the stellar disc with optical radius $R_{\rm opt}$ = 10 kpc, the total mass M_* = 4 × 10¹⁰ M_{\odot} , and the radial scale length r_d = 2.5 kpc;
- the gas disc with size R_g = 20 kpc and the total mass M_g = 0.8 × 10¹⁰ M_{\odot} ;
- − the dark matter halo with the mass inside of the optical radius $M_h = 20 \times 10^{10} M_{\odot}$ and the radial scale length a = 2.5 kpc;
- the spheroidal clumps of intergalactic gas (J = 1, 2, ..., 8) with a single cloud mass of $M_J = 0.2 \times 10^{10} M_{\odot}$, radius $R_J \approx 5$ kpc, and the total gas mass $8M_J$.

This gives the following conversion factors from dimensionless units in the numerical model into the physical units:

$$\ell_m = 4 \times 10^{10} M_{\odot}, \quad \ell_r = 10 \text{ kpc},$$

 $\ell_v \approx 131.5 \text{ km s}^{-1}, \quad \ell_t \approx 76 \times 10^6 \text{ years}.$ (9)

We will continue to use dimensionless characteristics in the text if their dimension is not explicitly indicated. Representing the results in a dimensionless form makes it possible to have solutions in a general form. The conversion factors ℓ_m , ℓ_r , ℓ_v , and ℓ_t give us a reference model. A more detailed description of the model and parallel implementation are given in Khrapov et al. (2021), Khoperskov et al. (2021), and Khrapov and Khoperskov (2017).

Two models of the main galaxy are considered. The stellar component of the first model does not contain a bulge, as in the case of late-type galaxies. The second includes the bulge with the following parameters in the King model:

- the bulge mass is $M_b = 2 \times 10^{10} M_{\odot}$,
- the radial scale of the bulge is $r_b = 0.8$ kpk,
- the density cut-off radius is $r_h^{(\text{max})} = 1.6$ kpc, after which the bulge density follows an exponential profile with scale $r_h^{(\exp)} = 0.3$ kpc.

This massive bulge is typical of early-type galaxies (Sa). The angular velocity of rotation of the disc $\Omega(r)$ increases significantly in the central region, where gravity from the bulge dominates. An increase in the degree of differential rotation of the disc $n = d \ln(\Omega)/d \ln(r)$ can create more favourable conditions for gas flow to the centre.

3 Simulation results

The general picture of the process of intergalactic gas accretion onto the galactic disc is shown in Figures 2 and 3. Time is given in dimensionless units ($t = 1 \rightarrow \ell_t = 76 \times 10^6$ years). The infall of gas clouds is accompanied by their rapid stretch along the trajectory, with the formation of a highly nonhomogeneous stream (Figure 2). The motion of the clouds chain starts in the region z > 0. The impact on the disc comes from the zone z < 0, which is due to the choice of the initial orbit and results in the collision with a retrograde velocity and subsequent counterrotation of the gas. The first collision of the accreting gas with the gaseous disc of the galaxy occurs at time $t \approx 2$ (~152 Myr). The counter-impact of gas flows leads to effective mixing and strong heating of the gas. We see the destruction of the galactic gaseous disc around $t \ge 4$ (300 Myr).

We emphasize that we study the evolution of a rather strong gas flow with twice the mass of the initial gaseous galactic disc. The velocity of the intergalactic gas at the moment of impact is $|\mathbf{v}| \approx 2.5$ with components $v_r \approx -1.6$, $v_{o} \simeq -1.8$, and $v_{z} \simeq 0.8$ (Figure 1). Most of the galactic gas and the accreting matter are ejected outside the galaxy's stellar disc. The remaining part of the gas forms a relatively dense central core with a size of r = 0.4-0.6, which is caused by a significant loss of angular momentum during the impact. The consequences of the collision of gas flow at the initial stage lead only to weak bending oscillations of the stellar disc (Figure 2).

The subsequent stages of the evolution of the gaseous and stellar components are shown in Figure 3. The gas ejected due to the collision gradually returns to the galactic plane of the stellar disc (t = 6.6) and forms a retrograde rotating gas disc around the central core (t = 13.2). The radius of the new gaseous disc reaches $R_g \approx 0.8$ by the time t = 52.6 (~4 billion years). In addition, some of the gas forms a ring-like structure with counterrotation (1 < r < 2), inclined at an angle $\sim (30-60)^\circ$ relative to the plane of the stellar disc. Such polar gaseous rings are similar to those observed in some galaxies (Khoperskov et al. 2014) and reproduced in cosmological simulations (Snaith et al. 2012).

The following evolution of the stellar disc is accompanied by bending oscillations and the appearance of a strong precession, the inclination of its rotation plane reaches $\sim 45^{\circ}$ by the time t = 52.6. Thus, three gaseous components are highlighted as a result of accretion. First, an increased concentration of gas occurs in the central kiloparsec ($r \le 0.1$), which will be denoted by "core." The rotating gas within r < 1 forms a disc in the galactic plane of the stellar disc (the core is an integral part of this disc). Finally, the gas outside the optical radius (r > 1) has the shape of a rotating, slightly flattened ring, which is inclined to the plane of the galaxy.

Figure 4 shows the mass evolution in three kinematically distinct subsystems. The new gaseous disc lies in the region $r \le 1$ with a mass approximately three times larger than the initial mass in this region. Moreover, most of the gas in the disc is located in the core region (approximately $M_{\rm core}$ = 2/3 $M_{\rm disc}$ at later times). The formation of the outer polar ring requires more time and completed by $t \approx 45$. The core emerges very rapidly, and there is only very slow growth after t = 10 (760 Myr) due to viscous forces leading to a small accretion flow to the centre (see the slope of the red line in Figure 4). The formation of the ring and a new galactic gaseous disc ends after $t \approx 45$ (3.5 billion years).

The evolution of the system is followed by mixing of the initial gas of the galaxy with the intergalactic gas.

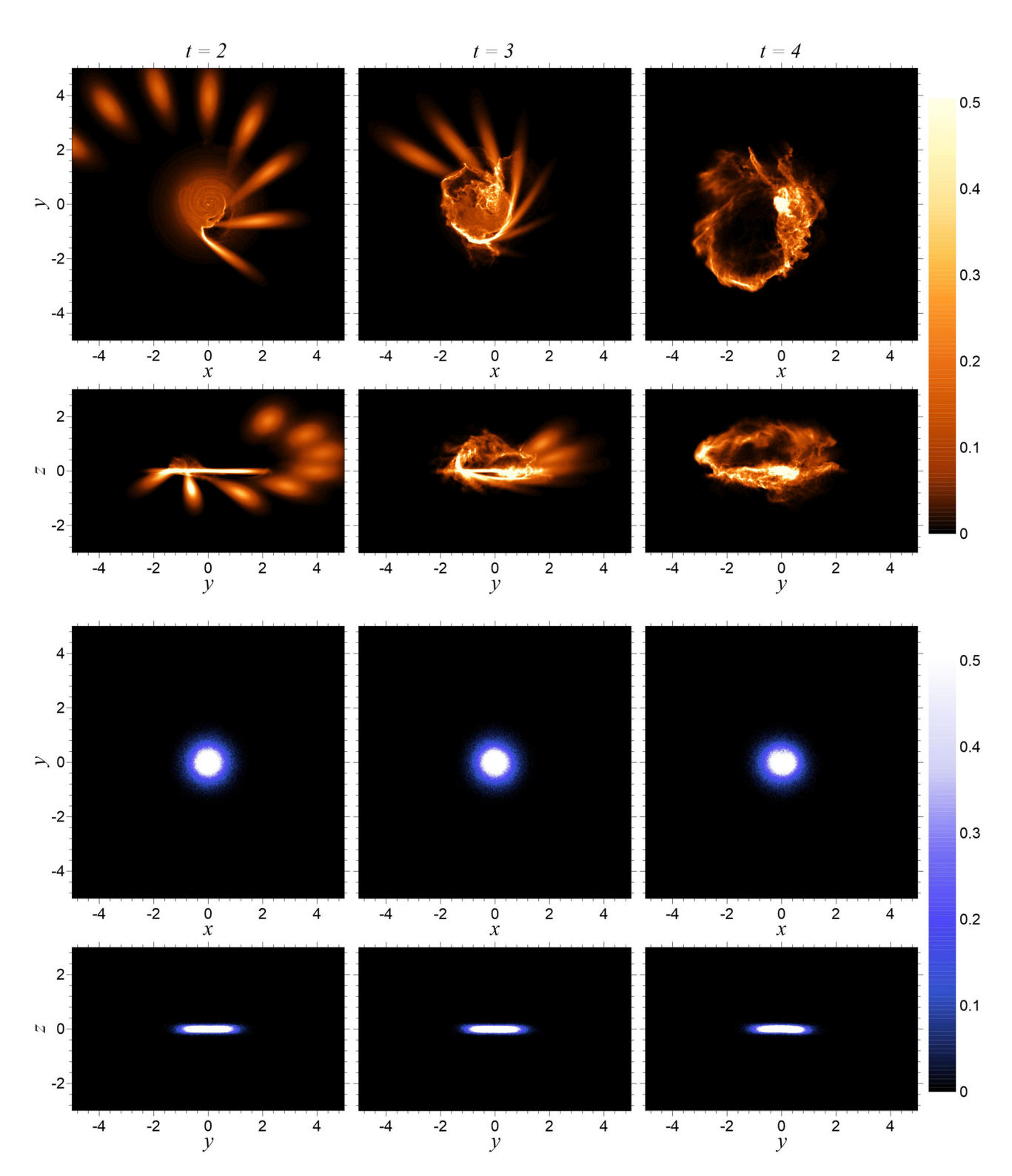


Figure 2: Surface density distributions of the gaseous (orange colour at the top) and stellar (blue colour at the bottom) components in various projections (XY and YZ) at the initial stages of collision of retrograde intergalactic gas with the disc galaxy (t = 2-4).

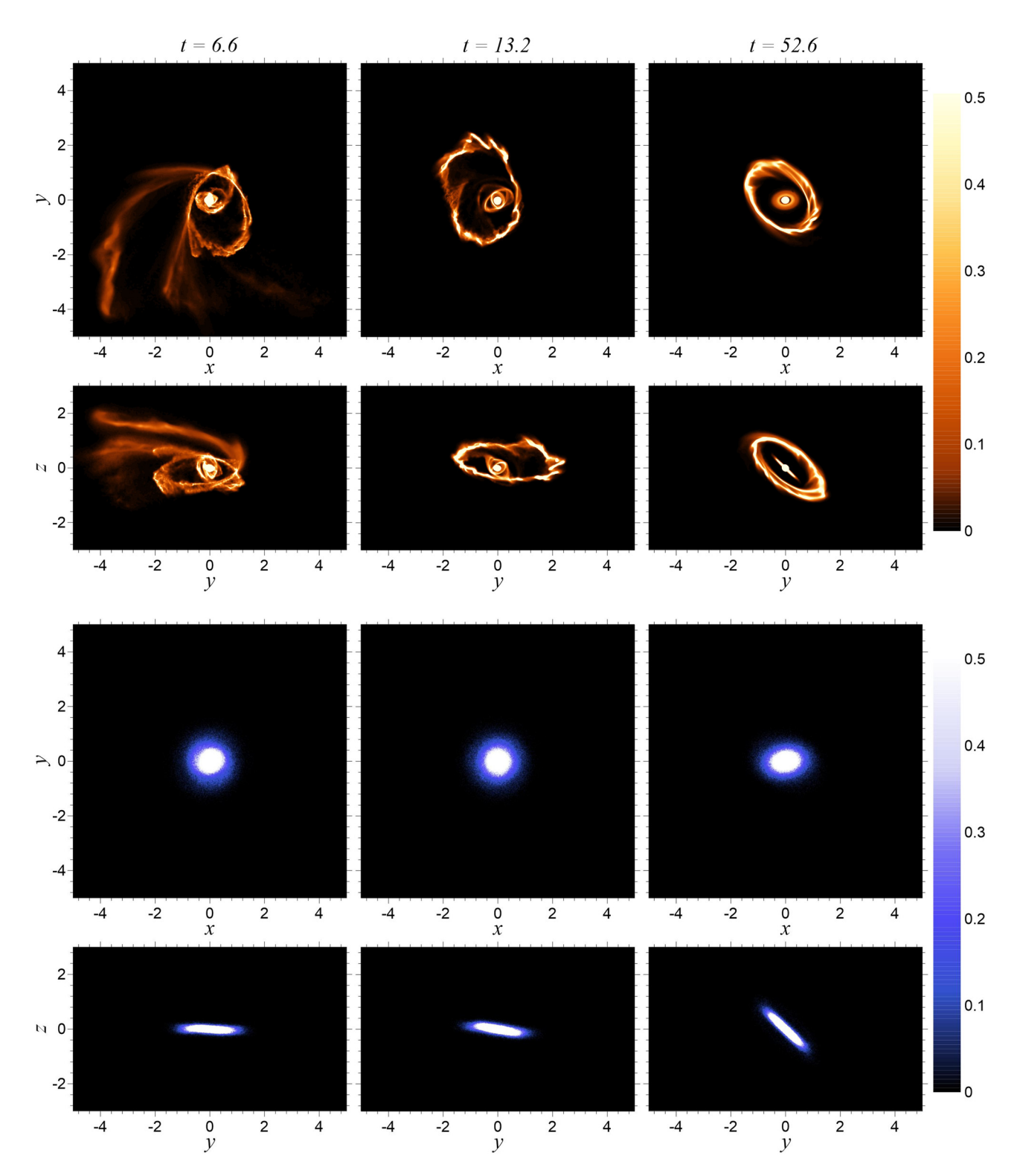


Figure 3: Surface density distributions of the gaseous (orange colour at the top) and stellar (blue colour at the bottom) components in various projections (XY and YZ) at the stage of formation of a new gaseous disc with opposite rotation in the precessing disc system (t = 6.6 - 52.6).

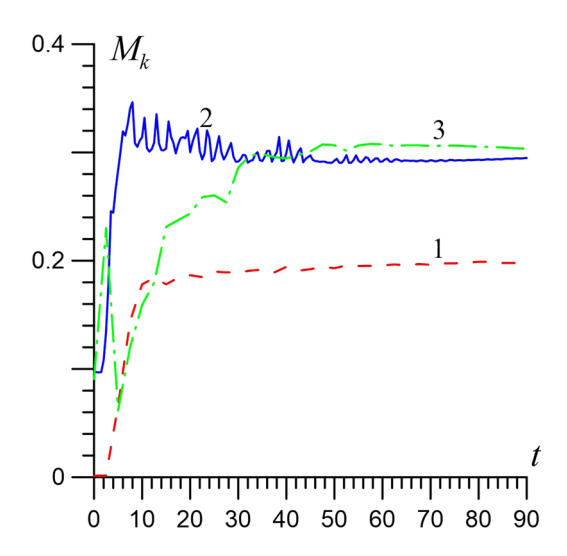


Figure 4: The evolution of the gas mass in the galactic centre $M_{\rm core}$ (r < 0.1, red line 1), in the disc $M_{\rm disc}$ (r < 1, blue line 2) and in the ring $M_{\rm ring}$ (1 < r < 2, green line 3) for the model with the retrograde gas and $\Theta_{\rm g} = 20^{\circ}$.

We highlight the fractions of the source gas in each of the three subsystems ($n_{\rm core}$, $n_{\rm disc}$, $n_{\rm ring}$) (Figure 5). The core and the disc masses include about 60–65% of the original gas of the galaxy after the establishment of a quasi-stationary picture. The intergalactic gas makes a contribution in the range of 35–40%. The ring is mainly made of intergalactic gas (more than 90% of the mass). There is less than 1% of the gas outside the two optical radii (r > 2) that kicked out to the larger distances as a result of the stream's impact into the disc.

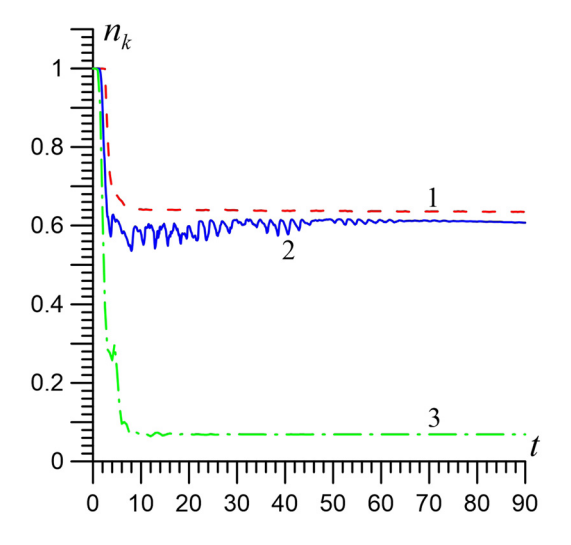


Figure 5: Dynamics of the mass fraction of the initial galactic gas in the core $n_{\rm core}$ (r < 0.1, red line 1), in the disc $n_{\rm disc}$ (r < 1, blue line 2) and in the ring $n_{\rm ring}$ (1 < r < 2, green line 3) for the retrograde gas infall model at $\Theta_{\rm g} = 20^{\circ}$.

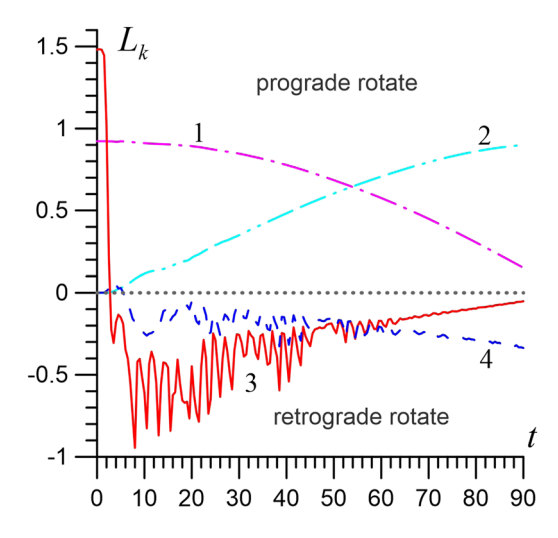


Figure 6: Evolution of the components L_z and L_y of the specific angular momentum for stellar disc (L_z , magenta line 1; L_y , light-blue line 2) and gaseous disc (L_z , red line 3; L_y , blue line 4) with $\Theta_g = 20^\circ$.

Understanding the complex 3D dynamics of multiple components is facilitated by calculating the angular momentum for each subsystem. Figure 6 shows the temporal variations of the two angular momentum components of the stellar disc, the gas disc, and the outer gas ring (Figure 3). The negative angular momentum corresponds to a retrograde rotation relative to the prograde rotation of the stellar disc (L > 0). Since the gas kinematics in these regions are very different, the gas component is divided into the inner part r < 1 and the outer zone 1 < r < 2. The external gas after the impact forms a kinematically isolated ring outside the plane of the stellar disc. The outer ring is tilted towards the stellar disc at an angle that changes slowly. Figure 7 shows the dynamics of the relative angular momentum of different components. The total angular momentum of the stellar subsystem varies within 1% over 7 Gyr (Figure 6), despite noticeable radial density redistributions in the stellar disc and its precession.

We observe a possible connection between the kinematic displacement of galactic components and the activity of the central black hole due to the inflow of a large amount of gas into the central kiloparsec. Figure 8 shows the time dependence of the gas mass in the centre of the computational domain, r < 1 kpc, for the retrograde and prograde gas infall simulations. Figures 4–7 contain simulation results in models without a bulge. Figure 8 also shows our calculations in bulge galaxy models for comparison.

The retrograde accretion simulation, already 400 Myr after the collision, increases the gas mass in the central region by about 100 times compared to the initial mass in the gaseous disc of the unperturbed galaxy. This is due to the fact that the infalling intergalactic gas mixes with the

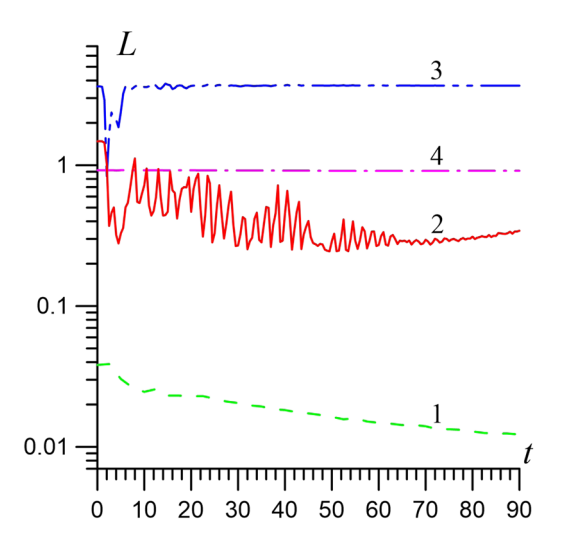


Figure 7: Specific angular momentum L vs time for the gas core (r < 0.1, green line 1), the gas disc (r < 1, red line 2), the gas ring (1 < r < 2, blue line 3) and the stellar disc (r < 1, magenta line 4) in the model with $\Theta_{\sigma} = 20^{\circ}$.

gas of the galaxy, and this mixture rapidly loses its angular momentum during the first crossing of the disc. The dense gaseous core also forms very quickly (Figure 2–7). The prograde infall of the gas does not result in mixing, and a massive gaseous core does not appear. The growth rate of the mass of such a core is very small over the entire simulation interval so that the final mass of the core is about two orders of magnitude smaller compared to the retrograde infall simulation.

Models with the bulge do not qualitatively change the results compared to the fall of gas onto the bulgeless galaxy. Curves 1 and 9 in Figure 8 were calculated for the bulgeless and bulge models, respectively, at $\Theta_g = 20^\circ$, which provides the highest rate of gas inflow into the centre of the galaxy. The model without the bulge gives the gas mass in the core only 10% less than with the bulge. This difference is possibly due to the central gradient of the disc rotation velocity. However, it must be taken into account that the addition of the massive bulge increases the mass of the entire stellar component and redistributes the gas in the disc along the radius during the evolution of the system. Cases of retrograde incidence (curves 8 and 10) also give similar results for the gas mass inside the core.

Therefore, the retrograde infall of gas on the galaxy provides a more efficient supply of gas in the galactic centre compared to the prograde infall, which connects the presence of kinematically displaced components in galaxies with AGN. A similar correlation was previously found for observed objects and numerical simulations in Starkenburg *et al.* (2019), Duckworth *et al.* (2020b), Gnilka

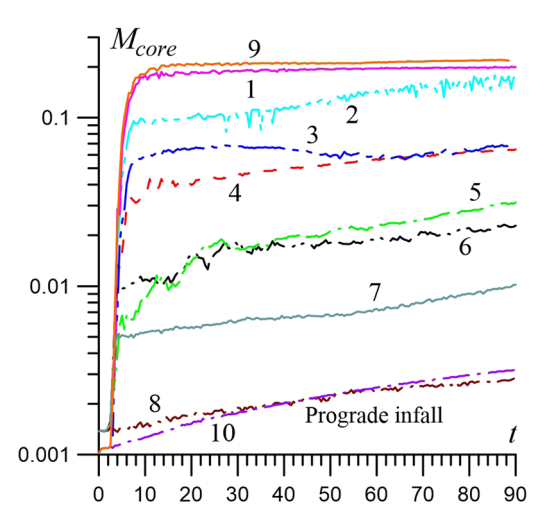


Figure 8: Influx of gas mass $M_{\rm core}$ into the inner region of the core (r < 0.1) at different angles Θ_g for retrograde infall of intergalactic gas into the disc of the bulgeless galaxy: $1 - \Theta_g = 20^\circ$; $2 - \Theta_g = 10^\circ$; $3 - \Theta_g = 5^\circ$; $4 - \Theta_g = 30^\circ$; $5 - \Theta_g = 40^\circ$; $6 - \Theta_g = 45^\circ$; $7 - \Theta_g = 60^\circ$. For comparison, the model with prograde infall $(8 - \Theta_g = 20^\circ)$ is also shown. Curves 9 and 10 describe galaxy models with the bulge at $\Theta_g = 20^\circ$ for retrograde and prograde infall, respectively.

et al. (2020), Raimundo (2021), Beom et al. (2022), Sil'chenko et al. (2022), and Raimundo et al. (2023). Our computational experiments confirm that the activity of galactic nuclei can be effectively enhanced due to the formation of counterrotating gas as a result of the accretion of the intergalactic medium. Mass growth within the central kiloparsec is quite sensitive to accretion conditions, which requires detailed studies (Figures 8 and 9).

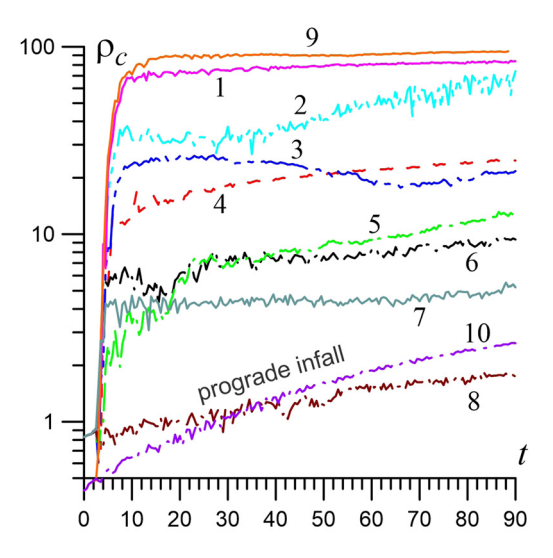


Figure 9: Evolution of the gas density in the galaxy centre ρ_c at different angles Θ_g in the model of retrograde infall of intergalactic gas. The colours, symbols, and lines are as in Figure 8.

The description provided above aligns seamlessly with the behaviour exhibited by the central gas density ρ_c , as illustrated in Figure 9. The outcomes depicted in Figures 8 and 9 underscore a pronounced dependency of gas supply efficiency to the galactic core on the angle of incidence of intergalactic flow. Notably, the most effective gas delivery to the central region is realized at an angle of $\alpha = 20^{\circ}$. A smaller infall angle, such as $\alpha = 10^{\circ}$, results in a halving of both M_{core} and ϱ_c . In contrast, an infall trajectory strictly within the galactic plane exhibits even lesser efficacy. This phenomenon can be attributed to the compromised conditions for the disruption of the original gaseous disc. Furthermore, models employing an angle of incidence $\alpha > 20^{\circ}$ yield unsatisfactory outcomes due to the reduction in the relative velocity upon collision of the flows. For instance, a perpendicular infall does not lead to gas counterrotation at all.

Figure 10 shows changes in the angle of inclination of the outer gas ring (Θ_R) to the disc of the main galaxy at different gas incidence angles Θ_g . We calculate the orientations of the gas ring and the host galaxy disc based on the construction of the vector of the total specific angular momentum, assuming that this vector is perpendicular to the plane of the rotating ring. This simple method for estimating the orientation angles of a rotating system is especially convenient for SPH/N-body simulations. The condition $\Theta_R > \Theta_g$ is satisfied at any angle of incidence Θ_g after t > 10 = 760 million years (Figure 10). The outer rings are formed only after t > 10 in our models.

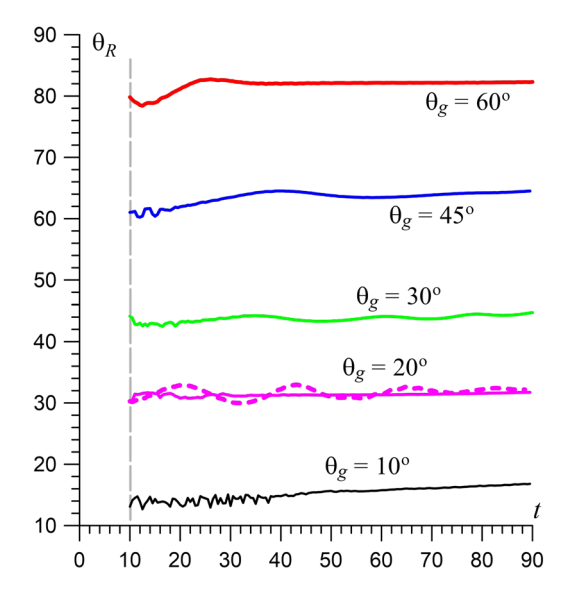


Figure 10: Dependences of the gas ring inclination angle (Θ_R) on time. The dashed line describes the behaviour of the model for $\Theta_g = 20^\circ$ with the bulge. The vertical grey line at t=10 approximately marks the end of the outer ring formation stage.

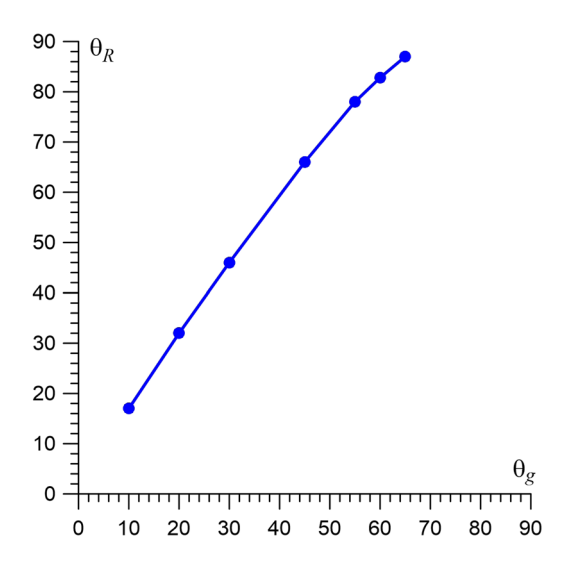


Figure 11: Relationship between the gas flow incidence angle (Θ_g) and the polar ring orientation angle at the end of the simulation (Θ_R) .

The ratio Θ_R/Θ_g at the end of the simulation weakly depends on the incident angle of the gas flow and is within $\Theta_R/\Theta_g \approx 1.4-1.6$. At incidence angles $\Theta_g > 60^\circ$, we have an almost polar ring with an angle $\Theta_R = (80-90)^\circ$ (Figure 11). Temporary changes in the functions $\Theta_R(t)$ are insignificant, which is a reflection of the law of conservation of angular momentum in the absence of relative precession of the ring and disc. The solid curves in Figure 10 are based on simulations with bulgeless models. We also show the simulation result of galaxy with bulge for comparison at $\Theta_g = 20^\circ$.

4 Conclusions and discussion

The formation process of counterrotating stellar and gaseous discs has been explored through numerical simulations focused on the accretion of gaseous intergalactic clouds. Our study concentrated on models where the mass of the accreting flow is twice that of the galactic gas. This choice of parameters establishes favourable conditions for the occurrence of counterrotation. As gas retrogradely falls into the central region of the gas-rich S-galaxy, it triggers the swift disintegration of the original gaseous disc. Subsequently, the formation of a new but smaller disc with opposing rotation becomes evident.

The robust interaction between nearly opposing streams of galactic and intergalactic gas results in the efficient dissipation of angular momentum. Within a sphere with a radius of 1 kpc, a mass comparable to that of the entire initial gaseous disc can accumulate due to this phenomenon. This gaseous core exhibits low angular momentum and a high

temperature, causing it to be predominantly supported by pressure forces. The presence of a supermassive black hole can induce radial flows that fuel central activity. The efficacy of gas inflow into the central zone, stemming from intergalactic cloud accretion, crucially hinges on the initial angle of incidence of the gas flow onto the disc (Θ_{σ}) . Our calculations reveal a non-monotonic pattern in the relationship between the mass $M_{\rm core}$ and Θ_g . The most substantial mass aggregation within 1 kpc occurs at an angle of approximately $\Theta_g \approx 20^\circ$. Elevating the angle of incidence to 40° leads to a nearly tenfold reduction in M_{core} .

DE GRUYTER

The prograde infall of intergalactic gas lacks the capacity to significantly disrupt the disc and does not induce a substantial inflow of gas within a radius of 1 kpc. In terms of gas mass accumulation within this range, this accretion mode only yields around 1% of what retrograde infall achieves.

The numerical simulations conducted to explore the dynamics of counterrotating stellar-gas discs encompass various stages of interaction with the descending intergalactic flow over a span of approximately 7 billion years. Prior work by Starkenburg et al. (2019) demonstrated the enduring nature of counterrotating gas and stars, persisting for around 2 billion years, following their formation in Illustris numerical simulations. Our approach is rooted in the qualitative dynamics exhibited by a single galaxy subjected to an accreting flow.

It is important to note that our models do not incorporate star formation and feedback resulting from galactic core activity. The presence of ionized gas at different distances from the disc plane, arising from multiple supernova explosions and the influence of OB stars (Vasiliev et al. 2022), is also absent in our model. Our primary focus revolves around the dynamic interaction between the intergalactic flow and the gas-rich disc galaxy.

An additional intriguing aspect arising from our simulations pertains to the development of outer gas rings oriented at an angle to the galactic plane. These structures resembling polar rings naturally emerge as a consequence of retrograde intergalactic gas infall onto the gas-rich galactic disc. While our primary focus is on scrutinizing the mechanism of gas delivery to the central region to fuel galactic nucleus activity, the formation of polar rings necessitates a distinct and dedicated analysis.

Let us note, however, some preliminary results related to outer ring structures. The angle between the ring and the main disc Θ_R is determined primarily by the angle of attack of the gas flow Θ_g in the model under consideration. We always get a ring with an angle $\Theta_R > \Theta_g$, so this ring is slightly different from the polar orientation at $\Theta_g \gtrsim 55^\circ$. The formation time of the outer ring occurs in approximately 1.5 billion years under the galaxy and gas filament parameters used. Further evolution is not accompanied by a change in the angle Θ_R . Smirnov *et al.* (2023) analysed the evolution of two rings in the Illustris TNG50 simulation, formed around massive galaxies due to interactions with companions. An interesting result of this work is the secular growth of the ring's inclination with a rate of 8°/Gyr. We see no change in the angle Θ_R in our simulations, which may be due to the symmetry of the dark halo shape. The question of the influence of the triaxial shape of the dark halo on the properties of the polar rings was discussed, e.g., in the works of Snaith et al. (2012), Combes (2014), Moiseev et al. (2015), and Zasov et al. (2017).

There are deviations of the rings from polar orientation ($\Theta_R = 90^\circ$) among the observed objects. The inclination of the ring in the galaxy PGC60020 is about 60° (Merkulova et al. 2012). The narrow inner ring in the galaxy PGC1806302 has a similar tilt angle (Finkelman et al. 2011). Various angles between the ring and the host disc are given for the sample of PRGs in the work of Mosenkov et al. (2022).

Given the intricacies of our simple model, which already encompasses numerous free parameters, such as initial masses, spatial distributions within each component, characteristics of the intergalactic flow orbit, and dark mass, the findings we have obtained warrant further expansion and deeper investigation in subsequent research.

Acknowledgments: The authors thank Sergey Khoperskov for helpful discussions of the results.

Funding information: This work was supported by the Russian Science Foundation (grant no. 23-71-00016, https:// rscf.ru/project/23-71-00016/). The research also relied on the shared research facilities of the HPC computing resources at the Lomonosov Moscow State University. The authors thank Sergey Khoperskov for helpful discussions of the results.

Author contributions: All authors have accepted responsibility for the entire content of this manuscript and approved its submission.

Conflict of interest: Authors state no conflict of interest.

References

Barrera-Ballesteros JK, Garciiia-Lorenzo B, Falcón-Barroso J, van de Ven G, Lyubenova M, Wild V, et al. 2015. Tracing kinematic (mis)alignments in CALIFA merging galaxies. Stellar and ionized gas kinematic orientations at every merger stage. A&A. 582:A21. doi: 10.1051/ 0004-6361/201424935.

- Bassett R, Bekki K, Cortese L, Couch W. 2017. The formation of SO galaxies with counter-rotating neutral and molecular hydrogen. MNRAS. 471(2):1892-1909. doi: 10.1093/mnras/stx958.
- Bois M, Emsellem E, Bournaud F, Alatalo K, Blitz L, Bureau M, et al. 2011. The ATLAS3D project - VI. Simulations of binary galaxy mergers and the link with fast rotators, slow rotators and kinematically distinct cores. MNRAS. 416(3):1654-1679. doi: 10.1111/j.1365-2966.2011.19113.x.
- Bournaud F. Combes F. 2003. Formation of polar ring galaxies, A&A. 401(3):817-833. doi: 10.1051/0004-6361:20030150.
- Bekki K. 1997. Formation of polar-ring SO galaxies in dissipative galaxy mergers. ApJ. 490(1):L37-L40. doi: 10.1086/311008.
- Beom M, Bizyaev D, Walterbos RAM, Chen Y. 2022. SDSS IV MaNGA: characteristics of edge-on galaxies with a counter-rotating gaseous disc. MNRAS. 516(3):3175-3192. doi: 10.1093/mnras/stac1499.
- Bianchin M, Riffel RA, Storchi-Bergmann T, Riffel R, Ruschel-Dutra D, Harrison CM, et al. 2022. Gemini NIFS survey of feeding and feedback in nearby active galaxies - V. Molecular and ionized gas kinematics. MNRAS. 510(1):639-657. doi: 10.1093/mnras/stab3468.
- Brok M, Krajnović D, Emsellem E, Brinchmann J, Maseda M. 2021. Dynamical modelling of the twisted galaxy PGC 046832. MNRAS. 508(4):4786-4805. doi: 10.1093/mnras/stab2852.
- Butenko M, Khoperskov A, Khoperskov S. 2015. Galactic spiral pattern beyond the optical size induced by the triaxial dark halo. Balt Astron. 24(2):119-125. doi: 10.1515/astro-2017-0210.
- Butenko MA, Belikova IV, Kuzmin NM, Khokhlova SS, Ivanchenko GS, Ten AV, et al. 2022. Numerical simulation of the galaxies outer spiral structure: The influence of the dark halo non-axisymmetry on the gaseous disk shape. Math Phys Comput Simul. 25(3):73-83. doi: 10. 15688/mpcm.jvolsu.2022.3.5.
- Chen Y-M, Shi Y, Tremonti CA, Bershady M, Merrifield M, Emsellem E, et al. 2016. The growth of the central region by acquisition of counterrotating gas in star-forming galaxies. Nat. Commun. 7:13269. doi: 10.1038/ncomms13269.
- Combes F. 2014. Polar rings and the 3-dimensional shape of dark matter. arXiv: 1312.6475v1. doi: 10.48550/arXiv.1312.6475.
- Davis TA, Alatalo K, Sarzi M, Bureau M, Young LM, Blitz L, et al. 2011. The ATLAS3D project - X. On the origin of the molecular and ionized gas in early-type galaxies. MNRAS. 417:882-899. doi: 10.1111/j.1365-2966.2011.19355.x.
- Di Matteo P, Combes F, Melchior AL, Semelin B. 2008. Old stellar counterrotating components in early-type galaxies from elliptical-spiral mergers. A&A. 477(2):437-442. doi: 10.1051/0004-6361:20078296.
- Duckworth C, Starkenburg TK, Genel S, Davis TA, Habouzit M, Kraljic K, et al. 2020a. Decoupling the rotation of stars and gas - I. The relationship with morphology and halo spin. MNRAS. 492(2):1869-1886. doi: 10.1093/mnras/stz3575.
- Duckworth C, Starkenburg TK, Genel S et al. 2020b. Decoupling the rotation of stars and gas - II. The link between black hole activity and simulated IFU kinematics in IllustrisTNG. MNRAS. 495(4):4542-4547. doi: 10.1093/mnras/staa1494.
- Ebrová I, Łokas EL, Eliášek J. 2021. Galaxies with kinematically distinct cores in Illustris. A&A. 647:A103. doi: 10.1051/0004-6361/202039562.
- Finkelman I, Graur O, Brosch N. 2011. A candidate polar-ring galaxy in the Subaru deep field. MNRAS. 412(1):208-212. doi: 10.1111/j.1365-2966. 2010.17899.x.
- Franx M, Illingworth GD. 1988. A Counterrotating Core in IC 1459. ApJL. 327:L55. doi: 10.1086/185139.
- Gnilka CL, Crenshaw DM, Fischer TC, Revalski M, Meena B, Martinez F, et al. 2020. Gemini near-infrared field spectrograph observations of the Seyfert 2 galaxy Mrk 3: feeding and feedback on galactic and nuclear scales. ApJ. 893:A80. doi: 10.3847/1538-4357/ab8000.

- Hauschild R, Gabriel R, Storchi-Bergmann T, McDermid RM, Walsh JL, Tan J, et al. 2022. Gas inflows in the polar ring of NGC 4111: the birth of an AGN. MNRAS. 512(2):2556-2572. doi: 10.1093/mnras/stac634.
- Katkov IYu, Sil'chenko OK, Afanasiev VL. 2014. Decoupled gas kinematics in isolated S0 galaxies. MNRAS. 438(4):2798-2803. doi: 10.1093/ mnras/stt2365.
- Katkov IYu, Kniazev AYu, Sil'chenko OK Gasymov D. 2022. Star formation in outer rings of S0 galaxies, IV, NGC 254: A double-ringed S0 with gas counter-rotation. A&A. 658:A154. doi: 10.1051/0004-6361/ 202141934
- Katkov I, Gasymov D, Kniazev A, Gelfand J, Rubtsov E, Chilingarian I, et al. 2023. Probing a galaxy assembly history for the counter-rotating disk galaxy PGC 66551. arXiv:2305.01719.
- Khoperskov AV, Khrapov SS, Sirotin DS, 2024, Formation of transitional cE/UCD galaxies through massive disc to dwarf galaxy mergers. Galaxies. 12(1):1. doi: 10.3390/galaxies12010001.
- Khoperskov SA, Moiseev AV, Khoperskov AV, Saburova AS. 2014. To be or not to be oblate: the shape of the dark matter halo in polar ring galaxies. MNRAS. 441(3):2650-2662. doi: 10.1093/mnras/stu692.
- Khoperskov S, Zinchenko I, Avramov B, Khrapov S, Berczik P, Saburova A, et al. 2021. Extreme kinematic misalignment in IllustrisTNG galaxies: the origin, structure, and internal dynamics of galaxies with a large-scale counterrotation. MNRAS. 500(3):3870-3888. doi: 10.1093/mnras/staa3330.
- Khrapov S, Khoperskov A. 2017. Smoothed-particle hydrodynamics models: implementation features on GPUs. Commun Comput Inf Sci. 793:266-277. doi: 10.1007/978-3-319-71255-0 21.
- Khrapov S, Khoperskov A, Korchagin V. 2021. Modeling of spiral structure in a multi-component milky way-like galaxy. Galaxies. 9(2):A29. doi: 10.3390/galaxies9020029.
- Krajnović D, Emsellem E, Cappellari M, Alatalo K, Blitz L, Bois M, et al. 2011. The ATLAS3D project - II. Morphologies, kinemetric features and alignment between photometric and kinematic axes of earlytype galaxies. MNRAS. 414(4):2923-2949. doi: 10.1111/j.1365-2966. 2011.18560.x.
- Li S-I, Shy Y, Bizyaev D, Duckworth C, Yan R-b, Chen Y-m, et al. 2021. The impact of merging on the origin of kinematically misaligned and counter-rotating galaxies in MaNGA. MNRAS. 501(1):14-23. doi: 10.1093/mnras/staa3618.
- Lu S, Xu D, Wang Y, Chen Y, Zhu L, Mao S, et al. 2021. Hot and counterrotating star-forming disc galaxies in IllustrisTNG and their realworld counterparts. MNRAS. 503(1):726-742. doi: 10.1093/mnras/ stab497.
- Mapelli M, Rampazzo R, Marino A. 2015. Building gas rings and rejuvenating S0 galaxies through minor mergers. A&A. 575:A16. doi: 10.1051/0004-6361/201425315.
- Merkulova OA, Karataeva GM, Yakovleva VA, Burenkov AN. 2012. PGC 60020: a polar-ring galaxy. Astrophys Bull. 67(4):374–384. doi: 10.1134/S1990341312040037.
- Moiseev AV. 2008. Warped polar ring in the Arp 212 galaxy. Astrophys Bull. 63(3):201-215. doi: 10.1134/S1990341308030012.
- Moiseev AV, Smirnova KI, Smirnova AA, Reshetnikov VP. 2011. A new catalogue of polar-ring galaxies selected from the Sloan digital sky survey. MNRAS. 418(1):244-257. doi: 10.1111/j.1365-2966.2011.19479.x.
- Moiseev A, Khoperskov S, Khoperskov A, Smirnova K, Smirnova A, Saburova A, et al. 2015. Structure and kinematics of polar ring galaxies: new observations and estimation of the dark halo shape. Balt Astron. 24(1):76-83. doi: 10.1515/astro-2017-0205.
- Monaghan II. 1992. Smoothed particle hydrodynamics, A&A, 30:543-574. doi: 10.1146/annurev.aa.30.090192.002551.

- Monaghan JJ. 2005. Smoothed particle hydrodynamics. Rep Prog Phys. 68:1703-1759. doi: 10.1088/0034-4885/68/8/R01.
- Mosenkov AV, Bahr SKH, Reshetnikov VP, Shakespear Z, Smirnov DV. 2023. The occurrence rate of galaxies with polar structures is significantly underestimated? arXiv:1107.1966. doi: 10.48550/arXiv.2311.03529.
- Mosenkov AV, Reshetnikov VP, Skryabina MN, Shakespear Z. 2022. Unveiling the Nature of Polar-ring Galaxies from Deep Imaging. Res Astron Astrophys. 22(11):115003. doi: 10.1088/1674-4527/ac8d82.
- Muller M, Charypar D, Gross M. 2003. Particle-based fluid simulation for interactive applications. Proceedings of the 2003 ACM SIGGRAPH/ Eurographics symposium on Computer Animation. Eurographics Association. 2003. p. 154-159.
- Nedelchev B, Coccato L, Corsini EM, et al. 2019. The properties of the kinematically distinct components in NGC 448 and NGC 4365. A&A. 623:A87. doi: 10.1051/0004-6361/201832840.
- Negri A, Ciotti L, Pellegrini S. 2014. The effects of stellar dynamics on the X-ray emission of flat early-type galaxies. MNRAS. 439:823-844. doi: 10.1093/mnras/stt2505.
- Osman O, Bekki K. 2017. Strong suppression of star formation and spiral arm formation in disc galaxies with counter-rotating gas discs. MNRAS. 471(1):L87-L91. doi: 10.1093/mnrasl/slx104.
- Pizzella A, Corsini EM, Beltrán JCV, Bertola F. 2004. Ionized gas and stellar kinematics of seventeen nearby spiral galaxies. A&A. 424:447-454. doi: 10.1051/0004-6361:20047183.
- Pizzella A, Morelli L, Corsini EM, Dalla Bonta E, Coccato L, Sanjana G. 2014. The difference in age of the two counter-rotating stellar disks of the spiral galaxy NGC 4138. A&A. 570:A79. doi: 10.1051/0004-6361/201424746.
- Proshina IS, Kniazev AYu, Sil'chenko OK. 2016. Counter-rotating gas disk in the S0 galaxy IC 560. Astron Lett. 42(12):783-789. doi: 10.1134/ S1063773716120057.
- Raimundo SI. 2021. External gas accretion provides a fresh gas supply to the active S0 galaxy NGC 5077. A&A. 650:A34. doi: 10.1051/0004-6361/202040248.
- Raimundo SI, Malkan M, Vestergaard M. 2023. An increase in black hole activity in galaxies with kinematically misaligned gas. Nat Astron. 7:463-472. doi: 10.1038/s41550-022-01880-z.
- Reshetnikov VP, Faundez-Abans M, de Oliveira-Abans M. 2011. Polar-ring galaxies: New candidates and statistics. Astron Lett. 37(3):171-180. doi: 10.1134/S1063773711030042.

- Reshetnikov VP, Mosenkov AV. 2019. New candidates to polar-ring galaxies from the Sloan digital sky survey. MNRAS. 483(2):1470-1480. doi: 10.1093/mnras/sty3209.
- Reshetnikov V, Sotnikova N. 1997. Global structure and formation of polar-ring galaxies. A&A. 325(3):933-942. doi: 10.48550/arXiv.astroph/9704047.
- Saburova AS, Chilingarian IV, Katkov IY, Egorov OV, Kasparova AV, Khoperskov SA, et al. 2018. A Malin 1 'cousin' with counter-rotation: internal dynamics and stellar content of the giant low surface brightness galaxy UGC 1922. MNRAS. 481(3):3534-3547. doi: 10. 1093/mnras/sty2519.
- Sil'chenko OK, Moiseev AV, Gusev AS, Kozlova DV. 2022. Kinematics and Origin of Gas in the Disk Galaxy NGC 2655. Astrophys Bull. 77(4):397-406. doi: 10.1134/S1990341322040137.
- Smirnov DV, Mosenkov AV, Reshetnikov VP. 2023. Polar-ring galaxies in the Illustris TNG50 simulation, arXiv:2310.18597.
- Smirnov DV, Reshetnikov VP. 2020. Active Galactic Nuclei among Polar-Ring Galaxies. Astron Lett. 46(8):501-508. doi: 10.1134/ S1063773720080046.
- Snaith ON, Gibson BK, Brook CB, Knebe A, Thacker RJ, Quinn TR, et al. 2012. The halo shape and evolution of polar disc galaxies. MNRAS. 425(3):1967-1979.
- Starkenburg TK, Sales LV, Genel S, Manzano-King C, Canalizo G, Hernquist L. 2019. On the origin of star-gas counterrotation in low-mass galaxies. ApJ. 878:A143. doi: 10.3847/ 1538-4357/ab2128.
- Titov AV, Khoperskov AV. 2022. Numerical modeling of the collisions of spheroidal galaxies: mass loss efficiency by Baryon components. Vestnik St. Petersburg University. Mathematics. 55(1):124-134. doi: 10.1134/S1063454122010149.
- Vasiliev EO, Drozdov SA, Shchekinov YA. 2022. Halpha emission from gaseous structures above galactic discs. Open Astron. 31(1):99-105. doi: 10.1515/astro-2022-0012.
- Zasov AV, Saburova AS, Khoperskov AV, Khoperskov SA. 2017. Dark matter in galaxies. Physics-Uspekhi. 60(1):3-39. doi: 10.3367/UFNe.2016.03.
- Zinchenko IA. 2023. Gas and stellar kinematic misalignment in MaNGA galaxies: What is the origin of counter-rotating gas? A&A. 674:id.L7. doi: 10.1051/0004-6361/202346846.